Weierstraß-Institut
für Angewandte Analysis und Stochastik

im Forschungsverbund Berlin e.V.

Preprint ISSN 0946 – 8633

Stochastic Eulerian model for the flow simulation in porous media

Dmitry Kolyukhin [1] and Karl Sabelfeld [1,2]

submitted: 3rd April 2003

[1] Weierstrass Institute for Applied Analysis and Stochastics
Mohrenstraße 39
D – 10117 Berlin
Germany
E-Mail: sabelfeld@wias-berlin.de

[2] Institute of Computational Mathematics and Mathematical Geophysics
Russian Acad. Sci.
Lavrentieva str., 6
630090 Novosibirsk
Russia

No. 836
Berlin 2003

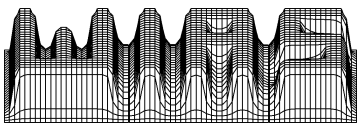

1991 *Mathematics Subject Classification.* 65C05, 76N20.

Key words and phrases. Hydraulic conductivity, Lognormal random field, small fluctuation, Darcy law, randomized spectral representation.

This work is supported by the Grant INTAS99-1501, and NATO Linkage Grant N 978912.

Edited by
Weierstraß-Institut für Angewandte Analysis und Stochastik (WIAS)
Mohrenstraße 39
D — 10117 Berlin
Germany

Fax: + 49 30 2044975
E-Mail: preprint@wias-berlin.de
World Wide Web: http://www.wias-berlin.de/

Abstract

This work deals with the stochastic flow simulation in statistically isotropic and anisotropic saturated porous media in 3D case. The hydraulic conductivity is assumed to be a random field with lognormal distribution. Under the assumption of smallness of fluctuations in the hydraulic conductivity we construct a stochastic Eulerian model for the incompressible flow as a divergenceless Gaussian random field with a spectral tensor of a special structure derived from Darcy's law.

A randomized spectral representation is then used to simulate this random field. Numerical results are compared with the analytical results obtained by the small pertrubation expansion. A series of test calculations confirmed the high accuracy and computational efficiency of the method. Comparisons with asymptotically exact results show a good agreement.

1 Introduction

The main difficulty in evaluation of pollutant transport in porous medium such as, for instance, aquifers is the extreme heterogeneity of the media. The parameters which locally describe the transport can be obtained in experiments, but they cannot be simply used to characterize the transport on large scales. Here we have a classical situation where there is a lack of knowledge on the local details of the spatial structure, but without this structure details it is not possible to describe the large scale behaviour. A natural approximation is based on the stochastic approach: the heterogeneities are modelled as random fields with given statistical properies. In hydrogeology this approach is often used, see, e.g., [6], [20] for the flow analysis in saturated zone, or [8], [15], [9], [3] for the transport of a dissolved pollutant in a saturated aquifer; see also overview in the books [5] and [10]. Stochastic approach allows for variations in other local properties, e.g., the hydraulic conductivity and the chemical adsorption coefficient (see [7], [2]), or the degradation constant (see [11]). An asymptotic analysis is undertaken in [16] when comparing two different averaging procedures.

To our knowledge, in the porous media transport, only one type of stochastic models was used, namely, the Random Displacement Method (RDM) for the hydrodynamic dispersion equation. It should be stressed that RDM can be applied only if the displacement covariance tensor is known (e.g., from measurements, or numerical simulation), and cannot be applied if the functionals of interest are evaluated at times comparable with the characteristic correlation scale of the flow. In contrast, the Lagrangian stochastic models based on the tracking particles in a random velocity field extracted from numerical solution of the flow equation (for brevity, we will call this model DSM, the Direct Simulation Method) are free of these limitations, but the computational resources required are vast. Therefore, it was quite suggestive to construct a Langevin type stochastic model which is

an approximation to DSM, and is written in the form of a stochastic differential equation for the position and velocity, see [14]. It is worth to mention that this approach is widely used in the atmospheric transport problems. The basis for the Langevin type approach comes from the Kolmogorov similarity theory of fully developed turbulence saying that in the inertial subrange the velocity structure tensor is a linear function in time. The linearity is the necessary condition to derive a Langevin type equation to mimic the behaviour of the real Lagrangian trajectories (see [12], [19]).

The main purpose of the present paper is to apply the random field simulation technique to the transport in porous medium, and to compare the results against the first order perturbation theory which is applicable for small fluctuations. The simulation of random fields is based on the spectral structure of the hydraulic conductivity. The results extracted from the numerical simulations are also useful to the parametrisation of the Lagra ngian stochastic model developed in [14]. A stochastic Eulerian and a combined Eulerian-Lagrangian models were used by us in [13] for the analysis of relative dispersion of two particles.

2 Formulation of the problem

We consider a steady flow through heterogeneous porous formation. For time- independent flow condition and saturated porous media the specific discharge is determined by the Darcy law:

$$\mathbf{q}(\mathbf{x}) = \theta(\mathbf{x})\mathbf{u}(\mathbf{x}) = -K(\mathbf{x})\nabla(\varphi(\mathbf{x}))$$

where $\mathbf{q}$ is the so-called Darcy's velosity, or specific discharge, $\mathbf{u}$ is the pore velosity, θ, the porosity, φ, the hydraulic potential $\varphi = \frac{p}{r_0}g + z$, p is the fluid pressure, z is the height, and K - is the hydraulic conductivity. The functions K and θ are key parameters of the flow. Experimental measurements show high heterogeneous behaviour of K in space with the following remarkable property: when considering K as a random field, its distribution is well approximated by the log-normal law. Therefore, in models, the hydraulic log-conductivity $Y = \ln K$ is commonly considered as a statistically homogeneous random field with gaussian distribution $N(m_Y, \sigma_Y)$. Here $m_Y = \langle Y \rangle$, and σ_Y is the standard deviation. We denote by $C_{YY}(\mathbf{r}) = \langle Y'(\mathbf{x})Y'(\mathbf{x}+\mathbf{r})\rangle$ the auto-correlation function, where $\mathbf{r}$ is the separation vector.

Moreover we assume first that Y is statistically homogeneous and isotropic with the exponential auto-correlation function

$$C_{YY}(r) = \sigma_Y^2 exp(-r/I_Y) \tag{1}$$

where $r = |\mathbf{r}|$, I_Y is a given correlation length. We will consider also the following anisotropic case

$$C_{YY}(\mathbf{r}) = \sigma_Y^2 \exp\left\{-\left(\frac{r_1^2}{I_1^2} + \frac{r_2^2}{I_2^2} + \frac{r_3^2}{I_3^2}\right)^{1/2}\right\} \tag{2}$$

where $\mathbf{r} = (r_1, r_2, r_3)$, and I_i, $i = 1, 2, 3$, is the correlation length in i-th direction.

We will deal also with a random field with gaussian form of the covariance:
$C_{YY}(r) = \sigma_Y^2 exp(-\frac{r^2}{l_Y^2})$.

The porosity θ is also often considered in some models as a random field. Howhever its variability is in the problems we tackle generally much smaller than that of K. We assume $\theta(x) = \theta = 1$.

Thus $\mathbf{q}$ is a random field obtained as the solution to the following diffusion equation:

$$\text{div}\,\mathbf{q} = \text{div}\,\{-K(\mathbf{x})\nabla(\varphi(\mathbf{x}))\} = \frac{\partial}{\partial x_i}\left(-K(\mathbf{x})\frac{\partial\varphi}{\partial x_i}\right) = 0. \tag{3}$$

Here and throughout the paper we use the summation convention on repeated indices. We assume small random pertrubation about mean values for the potential

$$\varphi = <\varphi> + \varphi' = H + h\ ,$$

and for the specific discharge components:

$$q_i = <q_i> + q_i', \quad i = 1, 2, 3\ .$$

Gelhar [10] studied the dependence between the value of σ_Y and the precision of head variance prediction. For one-dimensional flow he compared the approximate result based on the first-order approximation with exact head variance as it depends on the magnitude of σ_Y. At $\sigma_Y = 1$ the error is about 7% and increases up to over 50% at $\sigma_Y = 2$.

Using spectral methods Dagan [4] derived a second-order correction of the head covariances in 3D case. He noted that the first-order approximation is very robust and even for a log-conductivity variance equal to unity, the second-order correction of the head variance is smaller than 10% of first-order approximation. Thus, for small to moderate values of σ_Y^2, it is suggested that the first-order approximation is enough.

3 Spectrum of the specific discharge

We deal with statistically homogeneous random fields, hence we can use the Fourier-Stiltjes representations, in particular,

$$Y'(\mathbf{x}) = \int\int\int exp(i(\mathbf{k},\mathbf{x}))dZ_Y(\mathbf{k})$$
$$h(\mathbf{x}) = \int\int\int exp(i(\mathbf{k},\mathbf{x}))dZ_h(\mathbf{k})$$
$$q_j'(\mathbf{x}) = \int\int\int exp(i(\mathbf{k},\mathbf{x}))dZ_q(\mathbf{k}),$$

where $\mathbf{k} = (k_1, k_2, k_3)$ is the wave number vector, $\mathbf{x} = (x_1, x_2, x_3)$ is the position vector, and the integration is over three-dimensional wave number space.

The correlation tensor $\{B_{ij}\}$ and the spectral tensor $\{S_{ij}\}$ are related through the equality:

$$B_{ij}(\mathbf{r}) = \int_{R^3} S_{ij}(\mathbf{k})e^{i(\mathbf{r},\mathbf{k})}d\mathbf{k}\ .$$

The auto-covariance (1) has the spectrum

$$S_{YY}(k) = I_Y^3 \sigma_Y^2 / [\pi^2 (1 + I_Y^2 k^2)^2]$$

where $k = |\mathbf{k}|$, while the auto-covariance (2) has the spectrum

$$S_{YY}(\mathbf{k}) = \sigma_Y^2 I_1 I_2 I_3 / [\pi^2 (1 + I_1^2 k_1^2 + I_2^2 k_2^2 + I_3^2 k_3^2)^2] \ .$$

Note that the spectrum of the field with the gaussian covariance function has also a gaussian form:

$$S_{YY}(\mathbf{k}) = \frac{\sigma_Y^2 l_Y^3}{\pi^{5/2}} exp(-\frac{l_Y^2 k^2}{4}), \quad I_Y = l_Y \sqrt{\pi}/2 \ .$$

Assuming small pertrubations ($\sigma_Y^2 << 1$) Gelhar [9] evaluated the specific discharge spectrum using Darsy's law with isotropic hydraulic conductivity

$$q_i = -K(d\varphi/dx_i) = -K_G \, exp(Y')(d\varphi/dx_i) = -K_G[1 + Y' + Y'^2 + ...](dH/dx_i + dh/dx_i) \tag{4}$$

where $K_G = exp(< Y >)$, $\varphi = H + h$.

Under small pertrubation and dropping products of perturbed quantities, the mean-removed form of (4) is

$$q_i' = -K_G[Y'(dH/dx_i) + dh/dx_i]$$

and using the above Fourier-Stiltjes representation yields

$$dZ_{q_i} = K_G(J_i dZ_Y - ik_i dZ_h) \tag{5}$$

where $J_i = -dH/dx_i$ - is the mean hydraulic gradient in x_i direction, $\mathbf{J} = (J_1, J_2, J_3)$.

The following relation follows from (3) (e.g., see [1])

$$\nabla^2 h = J_i(dY'/dx_i). \tag{6}$$

Indeed, by (3) we find that

$$\frac{\partial^2 \varphi}{\partial {x_i}^2} + \frac{\partial \ln K}{\partial x_i} \frac{\partial \varphi}{\partial x_i} = 0; K \neq 0,$$

and taking the expected values we get

$$\frac{\partial^2 H}{\partial {x_i}^2} + \frac{\partial \langle Y \rangle}{\partial x_i} \frac{\partial H}{\partial x_i} + \left\langle \left[\frac{\partial Y'}{\partial x_i} \frac{\partial h}{\partial x_i} \right] \right\rangle = 0 \ .$$

After subtracting this from the original flow equation (3) we come to the following equation:

$$\frac{\partial^2 h}{\partial {x_i}^2} + \frac{\partial \langle Y \rangle}{\partial x_i}\frac{\partial h}{\partial x_i} + \frac{\partial Y'}{\partial x_i}\frac{\partial H}{\partial x_i} = \left\langle \left[\frac{\partial Y'}{\partial x_i}\frac{\partial h}{\partial x_i}\right] \right\rangle - \frac{\partial Y'}{\partial x_i}\frac{\partial h}{\partial x_i} \approx 0.$$

From this, due to the small fluctuation assumption, we ignore the products of fluctuations, and since the random field Y is homogeneous, $\frac{\partial \langle Y \rangle}{\partial x_i} = 0$, we come to the formula (6):

$$\frac{\partial^2 h}{\partial {x_i}^2} = J_i \frac{\partial Y'}{\partial x_i}.$$

From this one finds

$$dZ_h = -iJ_j k_j dZ_Y / k^2,$$

hence,

$$dZ_{q_i} = K_G(J_i - J_j k_i k_j / k^2) dZ_Y$$

which implies

$$S_{q_i q_j}(k) = \langle dZ_{q_i} dZ_{q_j} \rangle = K_G^2 J_m J_n (\delta_{im} - \frac{k_i k_m}{k^2})(\delta_{jn} - \frac{k_j k_n}{k^2}) S_{YY}(k) \ .$$

Using this spectrum we construct Monte Carlo simulation formulas for the specific discharge pertubation $\mathbf{q}'$, and hence the velocity $\mathbf{u}$. Under small perturbation assumptions, $< \mathbf{q} >= K_G \mathbf{J}$ (see [5]), so the velocity is modelled as $\mathbf{u}(x) = (K_G \mathbf{J} + \mathbf{q}'(x))/\theta$.

Note that the small perturbation assumption implies small values of σ_Y. In particular, the inequality $P(|exp(Y') - (1 + Y')|/exp(Y') < 0.1) > 0.97$ holds with $\sigma_Y < 0.2$.

4 Simulation of specific discharge pertrubation random field

The spectral tensor $S(\mathbf{k})$ of a general 3D incompressible (div $\mathbf{u} = 0$) homogeneous field has the form (e.g., see [17])

$$S_{ij}(\mathbf{k}) = b^2 \left(\delta_{ij} - \frac{k_i k_j}{k^2}\right) + \overline{a_i} a_j \left(1 - \frac{b^2}{a^2}\right), \ i, j = 1, 2, 3.$$

Here $\mathbf{a} = \mathbf{a}(\mathbf{k}) = (a_1(\mathbf{k}), a_2(\mathbf{k}), a_3(\mathbf{k}))^T$, $\mathbf{b} = \mathbf{b}(\mathbf{k}) = (b_1(\mathbf{k}), b_2(\mathbf{k}), b_3(\mathbf{k}))^T$ are vector functions such that the vectors $\mathbf{a}(\mathbf{k})$, $\mathbf{b}(\mathbf{k})$ and $\mathbf{k}$ are mutually orthogonal

$$(\mathbf{a}, \mathbf{b}) = (\mathbf{a}, \mathbf{k}) = (\mathbf{b}, \mathbf{k}) = 0, \quad (\mathbf{a}, \mathbf{b}) = \sum_{i=1}^{3} \overline{a_i} b_i,$$

and

$$a_i(-\mathbf{k}) = \overline{a_i(\mathbf{k})}, \quad b_i(-\mathbf{k}) = \overline{b_i(\mathbf{k})}, \quad i = 1, 2, 3.$$

A three-dimensional homogeneous incompressible random field is thus fully specified by two vector functions (in general, complex-valued) satisfying the above condithions. As mentioned in [17], p.30, this form can be transformed to

$$S_{ij}(\mathbf{k}) = \left(\delta_{jm} - \frac{k_j k_m}{k^2}\right)\left(\delta_{ln} - \frac{k_l k_n}{k^2}\right) F_{mn}(\mathbf{k}),$$

where $k = |\mathbf{k}|$, and $F_{mn}(\mathbf{k})$ is a simmetric tensor.

This makes possible to choose $\mathbf{b}(\mathbf{k}) = 0$, so that the entries of our spectral tensor $S(\mathbf{k})$ take the form

$$S_{ij}(\mathbf{k}) = a_i(\mathbf{k})a_j(\mathbf{k}) \tag{7}$$

where

$$a_i(\mathbf{k}) = K_G J_m(\delta_{im} - \frac{k_i k_m}{k^2})\left(S_{YY}(\mathbf{k})\right)^{1/2} \ .$$

Now we present simulation formulae for the incompressible random field with the spectral tensor $\{S_{ij}(\mathbf{k})\}$, see [18].

Let ξ_i and η_i be mutually independent random variables with zero mean and unit variance, and sample $\mathbf{k}$ according to $p(\mathbf{k}) = a^2(\mathbf{k})/\int_{R^3} a^2(\mathbf{k})d\mathbf{k}$, independently of ξ_i and η_i.

Let

$$\boldsymbol{\xi}'_i(\mathbf{a}) = \xi_i\, \mathbf{a}(\mathbf{k}) \ , \quad \boldsymbol{\eta}'_k(\mathbf{a}) = \eta_i\, \mathbf{a}(\mathbf{k}) \ .$$

Then we construct the vector random field

$$\mathbf{u}(\mathbf{x}) = \frac{1}{\sqrt{p(\mathbf{k})}}\left(\boldsymbol{\xi}'_i(\mathbf{a})\cos(\mathbf{k},\mathbf{x}) + \boldsymbol{\eta}'_i(\mathbf{a})\sin(\mathbf{k},\mathbf{x})\right) \ .$$

It is easy to verify that

$$\langle \boldsymbol{\xi}'_i(\mathbf{a})\boldsymbol{\xi}'_i(\mathbf{a})|\mathbf{k}\rangle = \langle \boldsymbol{\eta}'_i(\mathbf{a})\boldsymbol{\eta}'_i(\mathbf{a})|\mathbf{k}\rangle = S(\mathbf{k}),$$

and

$$\langle \boldsymbol{\xi}'_i(\mathbf{a})\boldsymbol{\eta}'_i(\mathbf{a})|\mathbf{k}\rangle = 0$$

by definition. Using these properties, it is possible to show that the random field $\mathbf{u}$ has the desired spectral tensor $\{S_{ij}(\mathbf{k})\}$.

We have described the simulation of a random field with zero mean $\overline{\mathbf{u}(\mathbf{x})} = 0$ and with a given spectral tensor $S(\mathbf{k})$, where no assumption about multidimensional distributions of the random field have been made. In the case of gaussian random fields the algorithm can be modified as follows. We simulate $i = 1, 2, \ldots N$ independent random fields with $S(\mathbf{k})$, then we set

$$\mathbf{u}^{(N)}(\mathbf{x}) = \frac{1}{\sqrt{N}}\sum_{i=1}^{N}\left[\frac{1}{\sqrt{p(\mathbf{k}_i)}}\left(\boldsymbol{\xi}'_i(\mathbf{a})\cos(\mathbf{k}_i,\mathbf{x}) + \boldsymbol{\eta}'_i(\mathbf{a})\sin(\mathbf{k}_i,\mathbf{x})\right)\right]$$

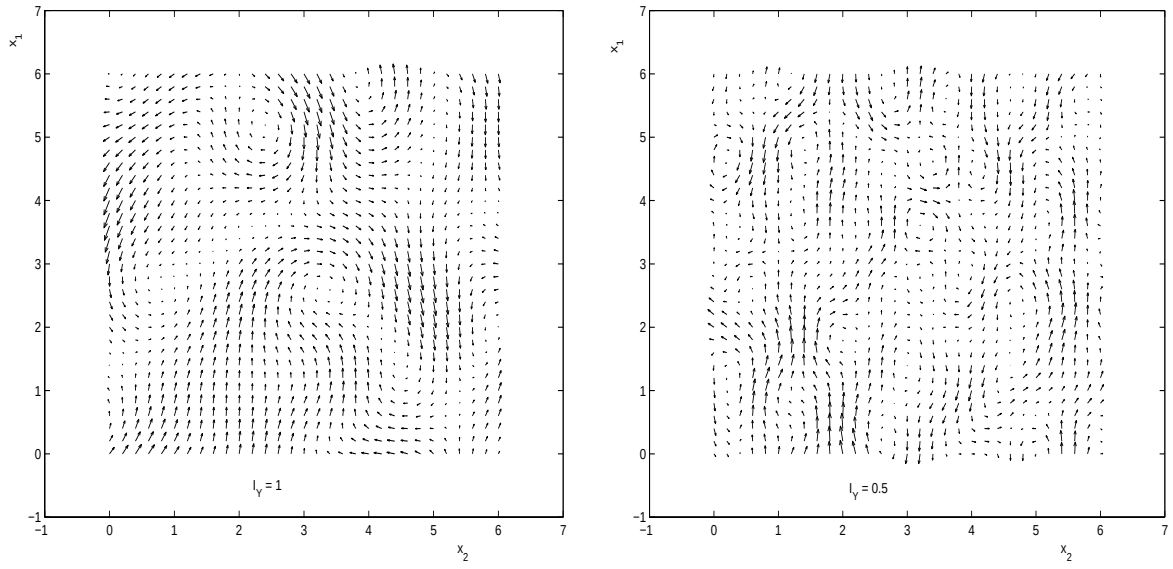

Figure 1: Samples of specific discharge pertrubation random fields q_1, q_2, for the isotropic hydraulic conductivity. Left picture: the correlation length $I_Y = 1$, right picture: $I_Y = 0.5$. The number of harmonics was $N = 100$.

where

$$\boldsymbol{\xi}_i'(\mathbf{a}) = \xi_i \, \mathbf{a}(\mathbf{k}) \ , \quad \boldsymbol{\eta}_i'(\mathbf{a}) = \eta_i \, \mathbf{a}(\mathbf{k})$$

and $\mathbf{k}_i$, ξ_i, η_i are all sampled independently.

The central limit theorem ensures, under some general assumption, that $\mathbf{u}^{(N)}(\mathbf{x})$ converges to an ergodic gaussian random field with the spectral tensor $S(\mathbf{k})$, as $N \to \infty$.

5 Testing the simulation procedure

In this section we present some results of simulation, in particular, we show examples of the discharge field samples with the given spectrum, and compare the simulation results against the exact solutions.

5.1 Samples examples

In Figure 1, left picture, we show one sample of specific discharge pertrubation random field q_1, q_2, in the region (x_1, x_2), x_3 fixed, for the correlation length $I_Y = 1$; right picture: the same as left, but for $I_Y = 0.5$.

Here we have chosen the gaussian form of the covariance: $C_{YY}(\mathbf{r}) = \sigma_Y^2 exp(-\frac{r^2}{l_Y^2})$ hence in the spectrum (7) the function S_{YY} has also a gaussian form: $S_{YY}(\mathbf{k}) = \frac{\sigma_Y^2 l_Y^3}{\pi^{5/2}} exp(-\frac{l_Y^2 k^2}{4})$, where $I_Y = l_Y\sqrt{\pi}/2$.

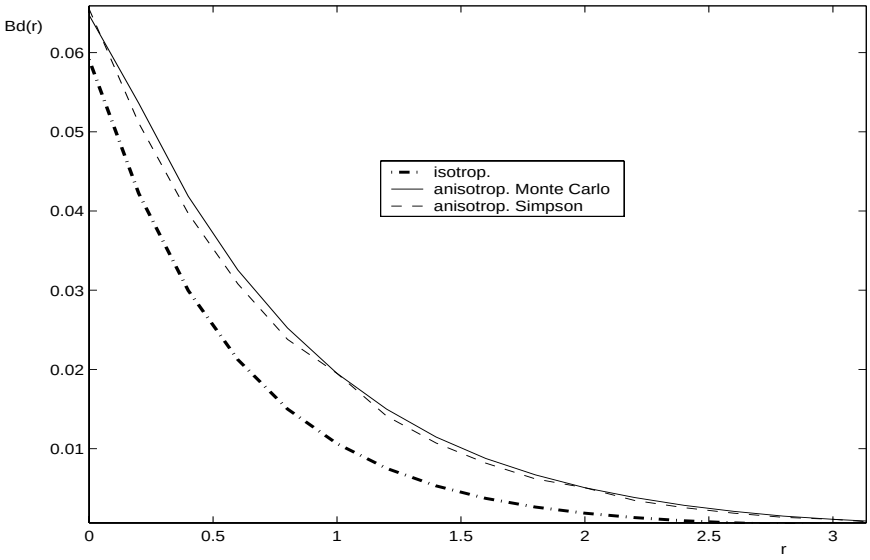

Figure 2: The functions $Bd(r) = Bd_{11}(r) + Bd_{22}(r) + Bd_{33}(r)$ for (I) Isotropic case: correlation length $I_Y = 1$, and (II) Anisotropic case: $I_1 = 1$, $I_2 = 2$, $I_3 = 3$.

5.2 Comparison with exact results

For testing our model we calculate the correlation functions

$$B_{ij}(\mathbf{r}) = \langle u_i(\mathbf{x}) u_j(\mathbf{x}+\mathbf{r}) \rangle$$

by using Monte Carlo simulation and compare them with results of numerical integration

$$B_{ij}(\mathbf{r}) = \int_{R^3} S_{ij}(\mathbf{k}) e^{i(\mathbf{r},\mathbf{k})} d\mathbf{k} \ . \tag{8}$$

The hydraulic conductivity $Y = ln(K)$ is assumed to be normal with the mean $\langle Y \rangle = 3.4012$ and covariances (1) or (2). The mean hydraulic gradient is fixed as $\mathbf{J} = (0.01, 0, 0)$, $\sigma_Y^2 = 1$. The expectation was calculated as an arithmetic mean over $N = 10^7$ samples, while the Simpson's rule was used to evaluate the integral (8).

Let us consider the correlations along the diagonal, i.e., let $Bd_{ij}(r) = \langle u_i(0,0,0) u_j(r,r,r) \rangle$.

We have considered two cases: (I) Isotropic case: correlation length $I_Y = 1$, and
(II) Anisotropic case: $I_1 = 1$, $I_2 = 2$, $I_3 = 3$.

In Figure 2 we plot the function $Bd(r) = Bd_{11}(r) + Bd_{22}(r) + Bd_{33}(r)$ for the isotropic and anisotropic cases. The error of calculations in the isotropic case is too small to see the difference between the curves (the lower curve). A small difference between the exact (Simpson's rule) and Monte Carlo results is seen in the anisotropic case (two upper curves). The same is true for the cross correlations Bd_{12} and Bd_{12} presented in Figure 3.

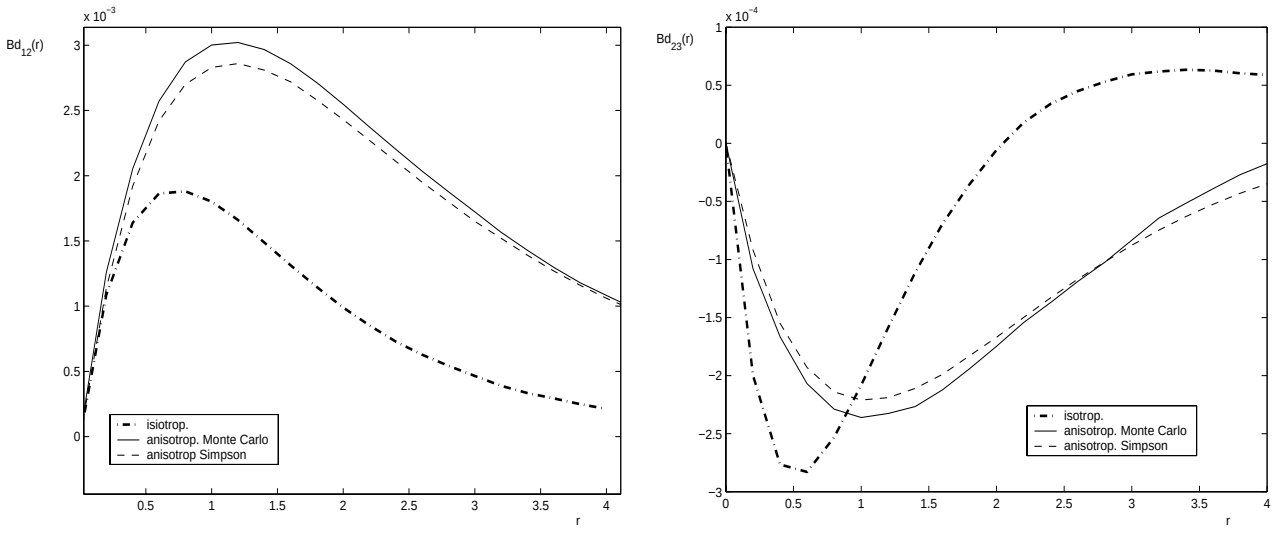

Figure 3: The functions $Bd_{12}(r)$ (left picture) and $Bd_{23}(r)$ (right picture) for the isotropic case: correlation length $I_Y = 1$.

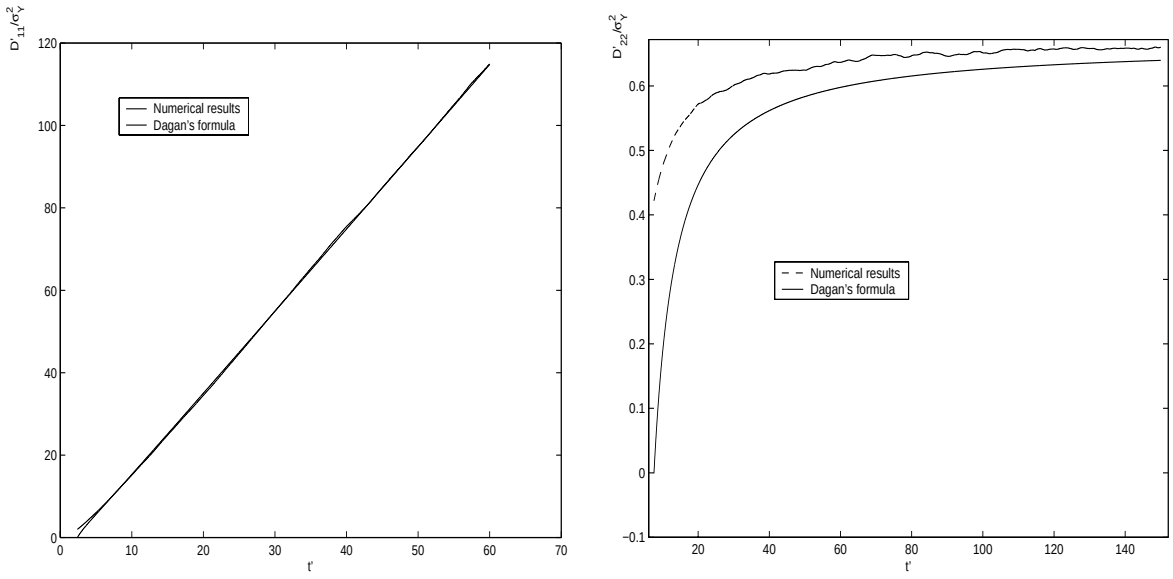

Figure 4: Monte Carlo calculations of functions D'_{11}/σ_Y^2 (left picture) and D'_{22}/σ_Y^2 (right picture) compared against the asymptotic formulae (10) and (11), respectively. The variance of Y: $\sigma_Y^2 = 0.01$.

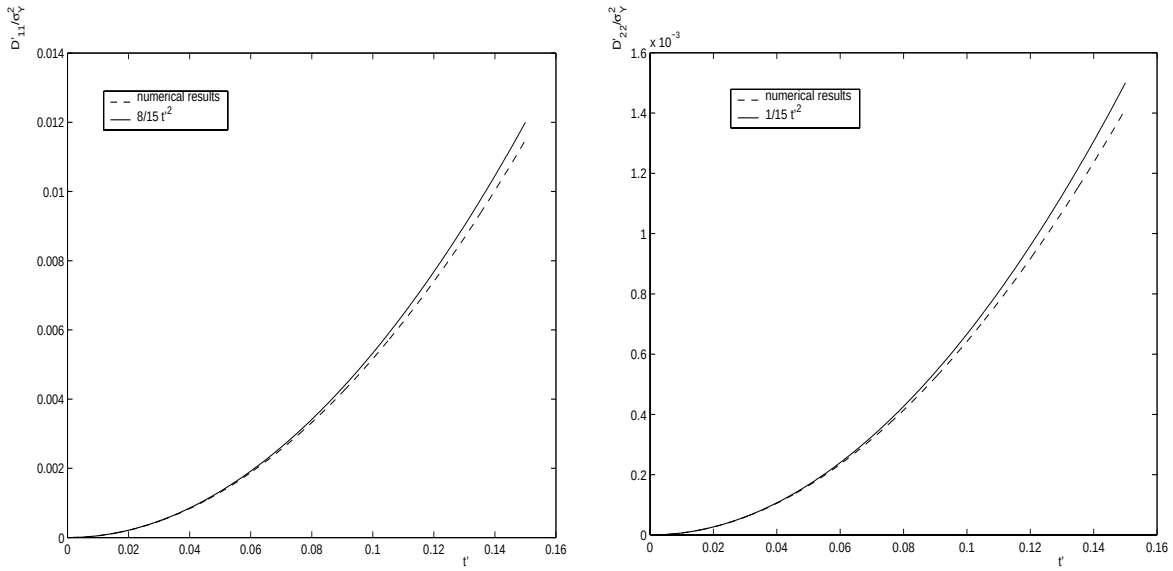

Figure 5: The same as in Figure 4, but for small values of t': the curves are compared against the results plotted according to the formulae (12).

6 Lagrangian statistical characterisics

In this section we present the results of numerical simulations for some Lagrangian statistical characteristics of the flow, and compare them with known exact or asymptotically exact results.

In simulations, $Y = ln(K)$ was taken as an isotropic gaussian random field with the mean $\langle Y \rangle = 3.4012$ and the exponentially decaying covariance (1) with the unit correlation length $I_Y = 1$. The mean hydraulic gradient is again fixed as $\mathbf{J} = (J_1, 0, 0)$, $J_1 = 0.01$.

Let us introduce a Lagrangian trajectory $\mathbf{X}(t) = (X_1(t), X_2(t), X_3(t))$ starting at a point $\mathbf{x}_0$ as a function satisfying the equation:

$$\frac{d\mathbf{X}}{dt} = \mathbf{u}(\mathbf{X}), \quad \mathbf{X}(0) = \mathbf{x}_0 \ . \tag{9}$$

It is assumed that the random velocity field $\mathbf{u}$ is smooth enough so that there exists a unique solution to (9) which is a vector random process with a mean $\langle \mathbf{X}(t) \rangle$. Then the displacement covariances are defined by

$$D_{ij}(t) = \langle (X_i(t) - \langle X_i \rangle(t))(X_j(t) - \langle X_j \rangle(t)) \rangle \ .$$

In what follows we deal with the normalized dispersions:

$$D'_{ij} = D_{ij}/I_Y^2, \quad i, j = 1, 2, 3,$$

and dimensionless time $t' = tU/I_Y$, where $U = K_G J_1$ (recall that we have assumed that $\theta = 1$).

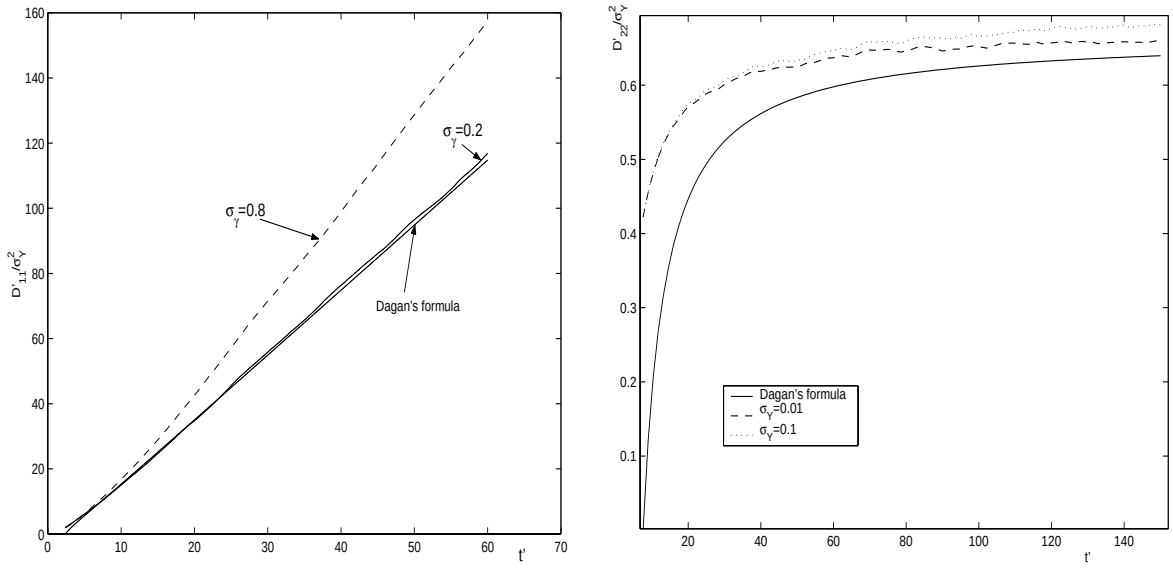

Figure 6: The same as in Figure 4, but for different values of σ_Y: $\sigma_Y = 0.2$ and 0.8 for D'_{11}/σ_Y^2 (left picture), and $\sigma_Y = 0.1$, 0.01 for D'_{22}/σ_Y^2 (right picture). Monte Carlo calculations are compared against the asymptotics (10).

In small pertrubation expansion Dagan [3] derived an asymptotical behaviour for the longitudial and transversal covariances D'_{11}, D'_{22} and D'_{33}. In the case of isotropic media for $t' >> 1$ he found

$$D'_{11}/\sigma_Y^2 = 2t' - 2[(8/3) - (4/t') - (8/t'^2) + ...] \tag{10}$$

for the longitudinal, and

$$D'_{22}/\sigma_Y^2 = D'_{33}/\sigma_Y^2 = 2[(1/3) - (2/t') - (4/t'^2) + ...] \tag{11}$$

for the transverse covariances, while for small values of t':

$$D'_{11}/\sigma_Y^2 = (8/15)t'^2 \ , \quad D'_{22}/\sigma_Y^2 = (1/15)t'^2 \ . \tag{12}$$

In Figure 4 the Monte Carlo calculations of functions D'_{11}/σ_Y^2 (left picture) and D'_{22}/σ_Y^2 (right picture) are compared against the results plotted according to asymptotic formulae (10) and (11), respectively. The variance of Y was taken as $\sigma_Y^2 = 0.01$, the relative error in the evaluation of D'_{11}/σ_Y^2 was less than 1%. The calculated and asymptotic curves in the left picture are practically coincident, so Dagan's formula works well in this time interval. The highest error in the evaluation of D'_{22}/σ_Y^2 was about 3% at $t' = 150$.

The same functions are shown in Figure 5 for small values of t': these curves are compared against the results plotted according to formulae (12). Again, there is a good agreement between the Monte Carlo calculations (Monte Carlo error varries between 3% and 5%) and the asymptotic formulae (12).

It is interesting to estimate how large should be the fluctuations to make the asymptotic formulae (10) and (11) (large times) not applicable. To this end, we compare these formulae with the results of numerical simulation for different values σ_Y^2. In Figure 6, left

picture, we plot the curves calculated for $\sigma_Y = 0.2, 0.3$ and 0.8 (Monte Carlo error less than 2%) and the asymptotics (10).

It is seen that $\sigma_Y^2 = 0.2, 0.3$ can be considered as the cases of small fluctuations, while $\sigma_Y^2 = 0.8$ results in a considerable deviation wich implies that the asymptotics fails.

The same kind of comparison is illustrated in the right picture of this figure, where D'_{22}/σ_Y^2 is presented for $\sigma_Y^2 = 0.01$ and $\sigma_Y^2 = 0.1$. These results show that the asymptotics for the transverse covariance D'_{22}/σ_Y^2 holds for much smaller fluctuations compared to the case of longitudinal covariance.

The Lagrangian trajectories (9) can be used to calculate the mean concentrtaions and other Lagrangian statistcis. As an example we plot in Figure 7 the trajectories of 500 particles started at $t' = 0$ and finished at $t' = 30$: we have taken $\sigma_Y^2 = 10^{-2}$ (left picture) and $\sigma_Y^2 = 1$ (right picture). The parameters were chosen as follows: $I_Y = 1$, isotropic case, $Y = ln(K)$ is normal with mean $< Y >= 3.4012$ and exponential covariance (1). The mean hydraulic gradient is fixed as $\mathbf{J} = (0.01, 0, 0)$.

In Figure 9 the influence of the correlation function decay on the longitudinal (left picture) and transversal (right picture) dispersions is illustrated. It is seen that the gaussian form of the correlation function leads to a faster dispersions both in longitudinal and transverse directions.

Further we consider the anisotropic case with $I_1 = I_2 = I_h, I_3 = I_v$, and the anisotropy ratio being defined as $e = I_v/I_h$. We use again the renormalized functions $D'_{ij} = D_{ij}/I_h^2, \quad i, j = 1, 2, 3$, and the dimensionless time $t' = t\,U/I_h$.

In Figure 10 the Monte Carlo calculations of the function D'_{11}/σ_Y^2 for $e = 0.2$ and $e = 1$, and the transvere dispersion D'_{22}/σ_Y^2 for $e = 0.2$, $e = 0.6$ and $e = 1$ are presented. The results agree well with the theoretical curves given in [5]. It is seen that the anisotropy has a much stronger influence on the transverse dispersion than on the longitudinal ones.

Important Lagrangian characteristic is the Lagrangian correlation tensor of velocity:

$$R_{ij}(\tau) = \langle [(u_i(X(t)) - \langle u_i(X(t))\rangle]\ [(u_j(X(t+\tau)) - \langle u_j(X(t+\tau))\rangle]\rangle$$

where X is a Lagrangian trjectory started at the time t.

We have calculated $R_{11}(\tau)$ and $R_{22}(\tau)$, - the Lagrangian correlation functions of the longitudinal and transverse velocities, respectively. In Figure 11 we plot these functions 1-normalized through dividing by $R_{ii}(0), \ \ i = 1, 2$ for two cases, (1) Left picture: for exponential covariance of the hydraulic conductivity, and (2) Right picture: for the gaussian covariance of the hydraulic conductivity. The longitudinal correlation function is positive, and it seems to decay exponentially, similar to the Eulerian correlation function. As to the transverse correlation function, there is (see the left picture) a clear interval betveen $\tau' = 1.83$ and $\tau' = 28$ where this function is negative, achieving its minimum value of about -0.1 at $\tau' = 3.51$. In the case (2) the behaviour is similar, but the negative values are in the interval $(1.32, 16)$, with the minimal value -0.23 at $\tau' = 2.14$.

Remakably, the transversal integral time scale defined as the integral of the transverse correlation function appears to be zero which makes impossible the application of the classical Taylor formula relating the dispersion with the integral of the correlation function. The long negative time correlations lead also to a trapping of particles and a non-Fickian behaviour of the transverse dispersion, see the right pictures of Figure 4 and Figures 6-10.

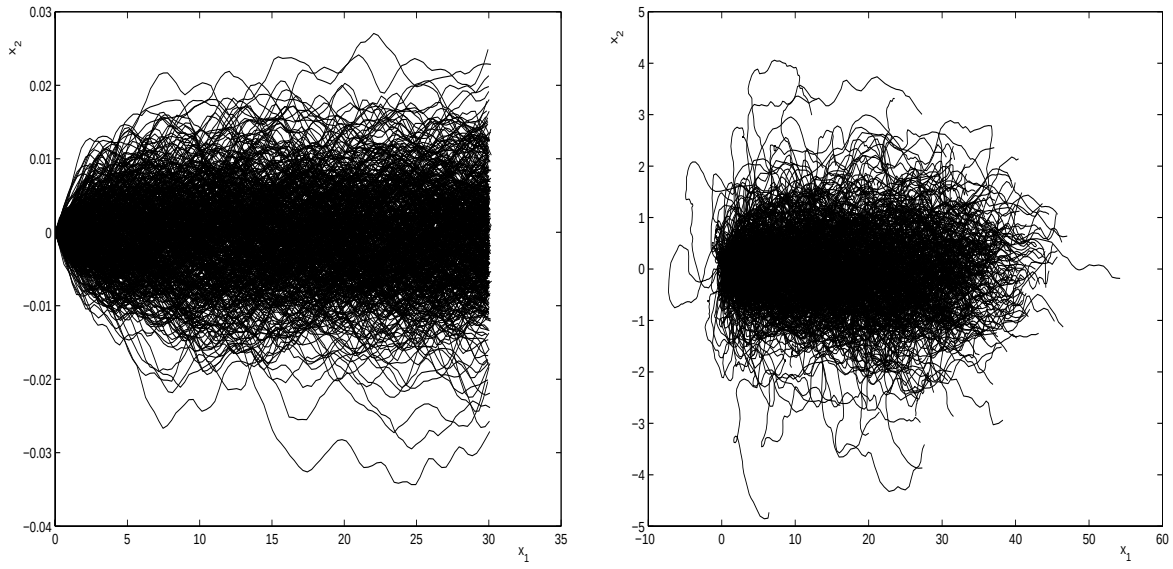

Figure 7: Trajectories of 500 particles started at $t' = 0$ at the origin, and finished at $t' = 30$: $\sigma_Y^2 = 10^{-2}$ (left picture) and $\sigma_Y^2 = 1$ (right picture).

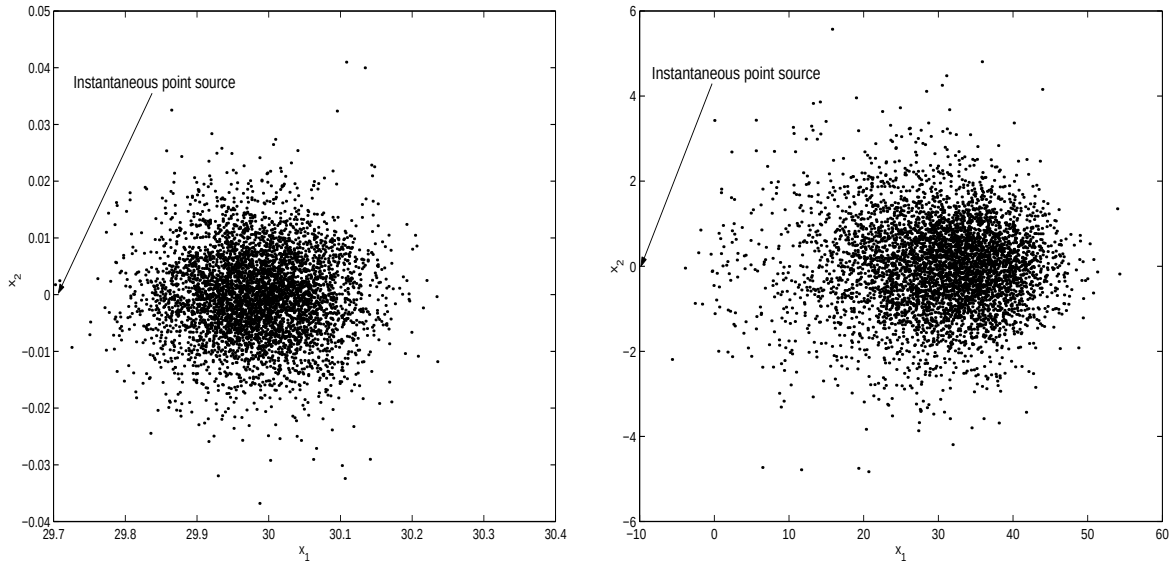

Figure 8: A cloud of 5000 particles ejected by an instantaneous point source at the origin, shown at the time instant $t' = 30$, $\sigma_Y^2 = 10^{-2}$ (left picture) and $\sigma_Y^2 = 1$ (right picture).

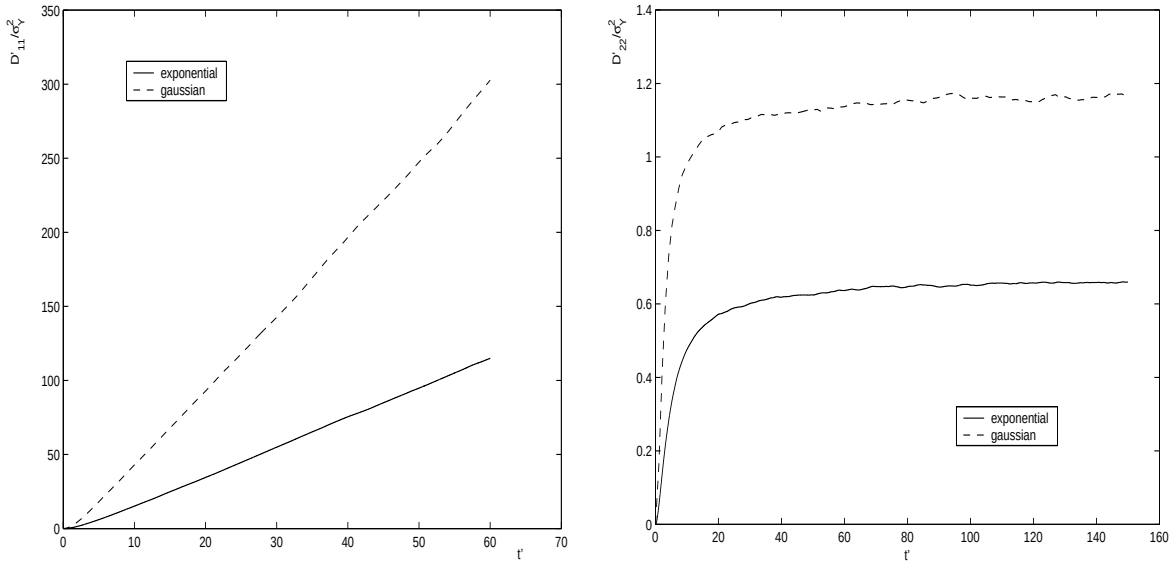

Figure 9: Illustration to the influence of the correlation function decay on the longitudinal (left picture) and transversal (right picture) dispersions.

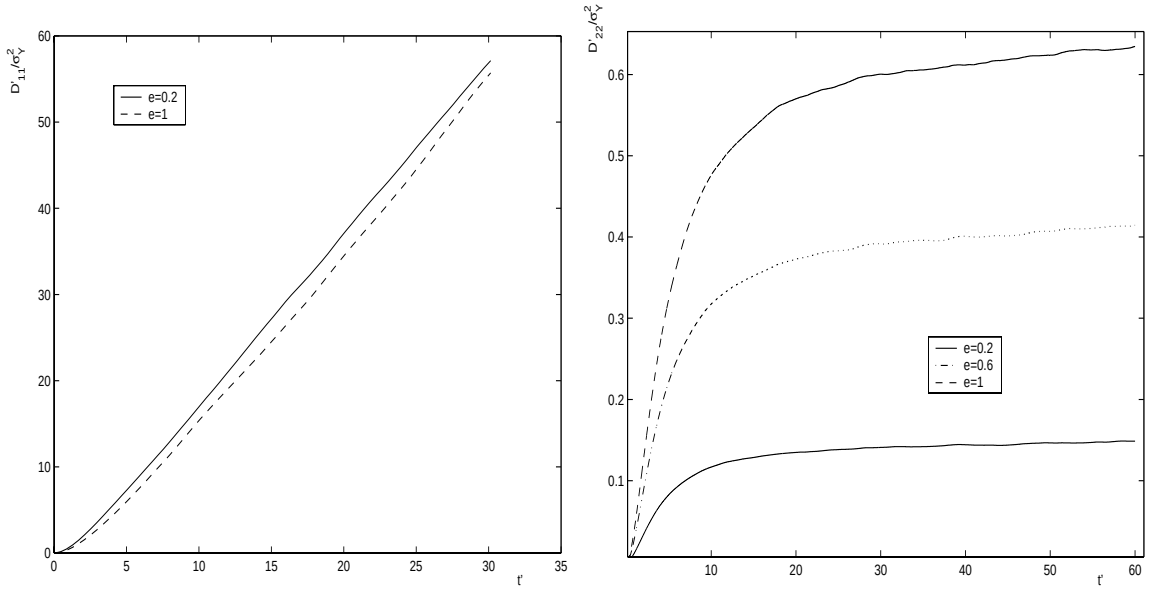

Figure 10: Anisotropic case: The function D'_{11}/σ_Y^2, for the anisotropy ratio $e = 1$ and 0.2 (left picture), and D'_{22}/σ_Y^2, for $e = 1, 0.6$ and 0.2 (right picture).

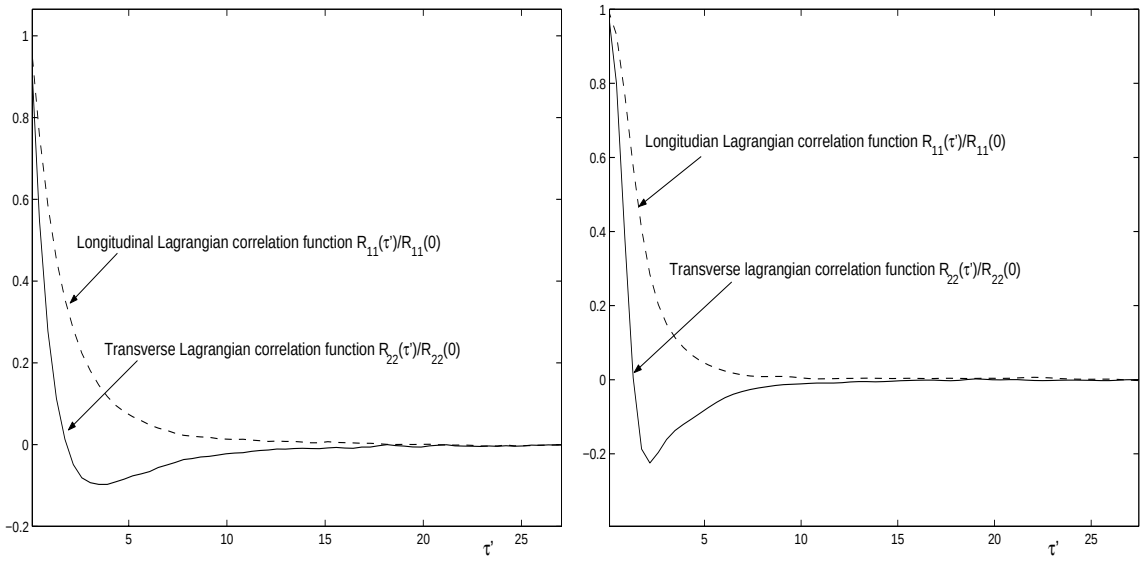

Figure 11: Lagrangian correlation functions of velocity: $\sigma_Y^2 = 0.01$, $\mathbf{J} = (0.01, 0, 0)$. Left picture: exponential covariance of the hydraulic conductivity; Right picture: gaussian covariance of the hydraulic conductivity;

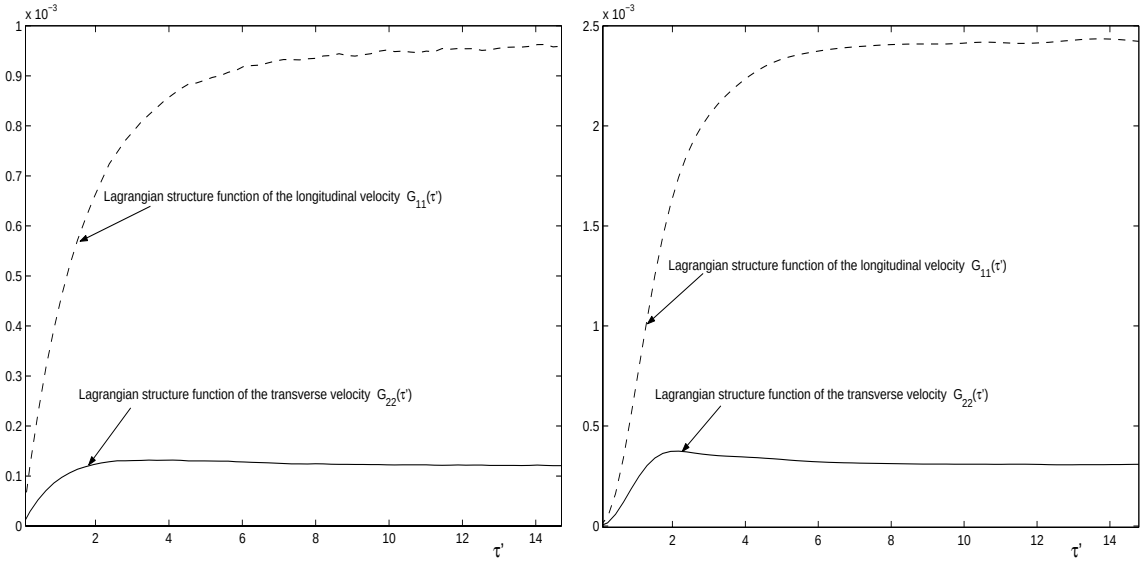

Figure 12: Lagrangian structure functions of velocity: the longitudinal and transverse components. Left picture: exponential covariance of the hydraulic conductivity; Right picture: gaussian covariance of the hydraulic conductivity;

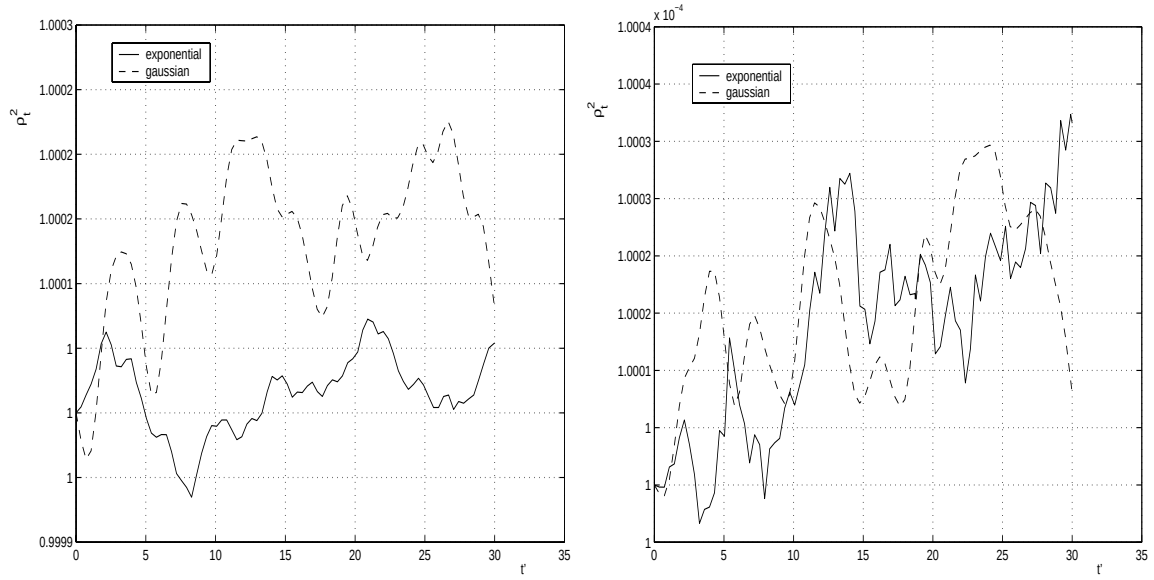

Figure 13: Squared transverse separation vector for two particles, initially separated by $\rho_0 = 1$ (left picture) and $\rho_0 = 0.01$ (right picture).

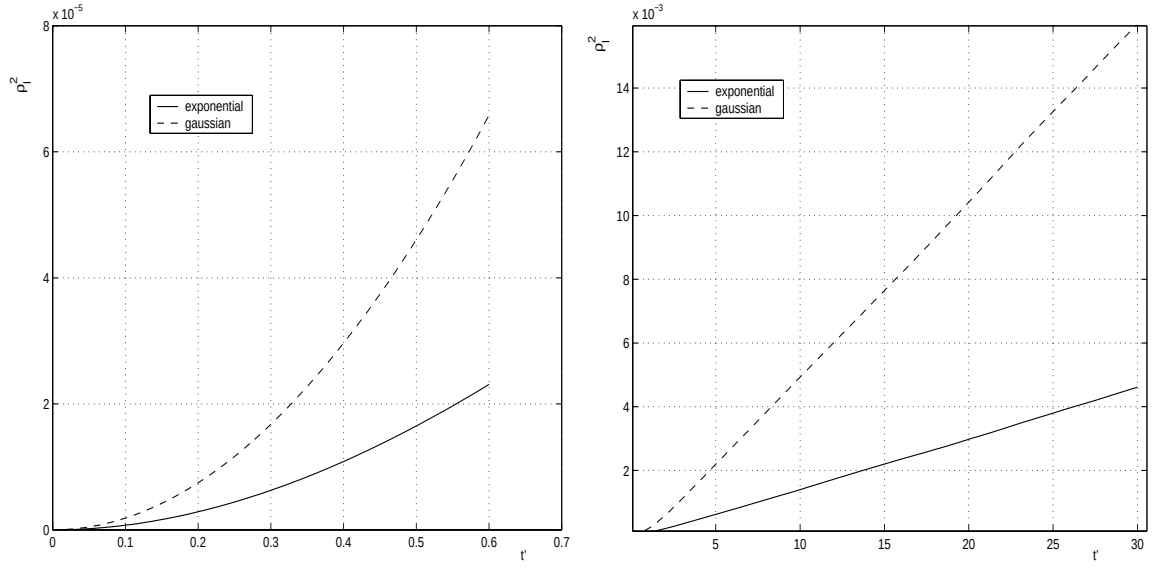

Figure 14: Squared longitudinal separation vector for two particles, initially separated by $\rho_0 = 1.$, for small times (left picture) and large times (right picture).

Important Lagrangian statistical characteristics are the Lagrangian velocity structure functions defined as [17]

$$G_{ij}(t) = \langle \Delta V_i(t)\, \Delta V_j(t) \,|\, \mathbf{X}(t_0) = \mathbf{x}_0; \rangle \ , \qquad i,j = 1,2,3 \ ,$$

where $\Delta V_i(t) = u_i(\mathbf{X}(t; t_0, \mathbf{x}_0)) - u_i(t_0)$. We have made the calculations of the longitudinal and transverse Lagrangian velocity structure functions, for two cases, when the correlation function of hydraulic conductivity is (1) exponential (see the left picture in Figure 12) and (2) gaussian (right picture in Figure 12). We do not show here the small time behaviour of these functions, which in the case (2) is quadratic in time while in the case (1) it is rather linear. In both cases a linear behaviour is seen in the time interval of about 1, while then it asymptotically approaches a constant as the time increases.

In the analysis of superdiffusion regime, and in the estimation of the concentration fluctuations the mean separation of two particles, $\boldsymbol{\rho}(t)$, plays a crucial role,

$$\boldsymbol{\rho}(t) = \mathbf{X}^{(1)}(t) - \mathbf{X}^{(2)}(t) \ ,$$

where $\mathbf{X}^{(1)}(t)$, $\mathbf{X}^{(2)}(t)$ are two Lagrangian trajectories initially separated by a vector $\boldsymbol{\rho}_0$. Thus the function $\boldsymbol{\rho}^2(t)$ depends generally on the time and on the initial separation $\boldsymbol{\rho}_0$. But it is heuristically clear that after a certain time instant the two particles will move independently hence the function $\boldsymbol{\rho}^2(t)$ should be linear. The main interest in the turbulence studies is here concerned with the question if there exists a time interval where the function $\boldsymbol{\rho}^2(t)$ depends cubically on time, like in the inertial subinterval of the fully developed turbulence, see [17]. It should be noted however that in our case we have to analyse the transverse and longitudinal components of $\boldsymbol{\rho}^2(t)$ separately, i.e.,

$$\boldsymbol{\rho}^2(t) = \boldsymbol{\rho}_t^2 + \rho_l^2,$$

where ρ_l is the longitudinal, and $\boldsymbol{\rho}_t$ is the transverse vector component of $\boldsymbol{\rho}(t)$ so that $\boldsymbol{\rho}_t^2 = \rho_{t1}^2 + \rho_{t2}^2$.

In Figure 13 we present $\boldsymbol{\rho}_t^2$, where the particles were initially separated by $\rho_0 = 1$ (left picture), and $\rho_0 = 0.01$ (right picture), for both exponential and gaussian correlation functions. Here the behaviour agrees with the existence of the negative Lagrangian correlation part: the function $\boldsymbol{\rho}_t^2$ is not monotonically increasing as we might have expect in analogy with the turbulent transport. However the longitudinal component, ρ_l^2 shows a classical "diffusion behaviour": it increases at small times quadratically (left picture of Figure 14), then switches to a power law, and ends up with a linear behaviour for large times which says us that the motion of the two particles is decorrelated in the longitudinal direction.

In conclusion we mention that different expansions of the desired Lagrangian statistical characteristics can be used, e.g., expansion in σ_Y for small fluctuations, or for large Pekle numbers, in Pe^{-1}, where Pe, the Pekle number is defined as $Pe = U\, I_Y / D_d$ with D_d, the dispersion at the pore-scale level. Of course, these two expansions are not independent, and one should carefully estimate the coefficients of the relevant expansions. In [5], an expansion in σ_Y leads generally to an artificial underestimation of the transverse dispersion (see Figures 4, 6 (right pictures) and 15, and formula (11)). However since it was assumed that the Pekle number is large, and hence the dispersion is dominated by the convective mechanism, the estimation is qualitatively not too crude.

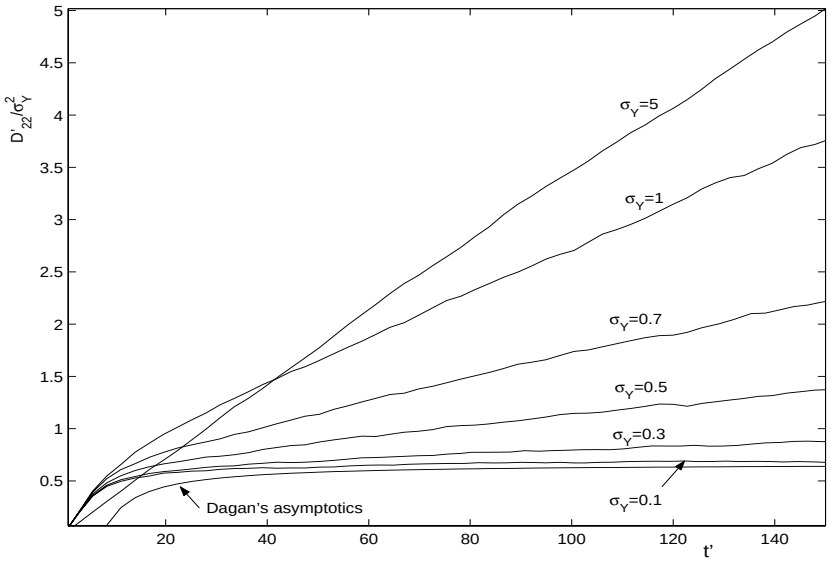

Figure 15: Transverse dispersion D'_{22}/σ_Y^2 for different values of the variance σ_Y.

In Figure 15 we show the transverse dispersion D'_{22}/σ_Y^2 for different values of σ_Y, and compare the curves with Dagan's asymptotics. This comparison can be considered only qualitatively, since the spectral tensor of the modeled velocity field is changing with the increase of the fluctuations. It is seen from Figure 15 that Dagan's asymptotics for large times is practically coincident with the curve with $\sigma_Y = 0.1$; the dispersion D'_{22}/σ_Y^2 increases with σ_Y. Note that the curve with $\sigma_Y = 5$. has a different behaviour: it is linearly increasing from the origin, and is down all the curves with smaller σ_Y which says about a superdiffusion regime in the time interval $(0, 14)$ for smaller values of σ_Y.

7 Conclusion

Stochastic Eulerian model for the flow in statisticaly isotropic and anisotropic porous media is constructed using spectral representational method. The randomized simulation approach developed in [18] is used to construct a divergenceless vector field with a given spectral tensor derived under the assumption of small hydraulic conductivity fluctuations. A series of test calculations confirmed the high accuracy and computational efficiency of the method. Comparisons with asymptotically exact results show a good agreement. This makes possible to find the applicability conditions of these asymptotics. Calculations of the longitudinal and transverse dispersions, the Lagrangian correlation functions and the distance between two particles have been carried out to extract the main statistical features of the flow. In particular a time interval with a superdiffusion regime in the transverse dispersion for small values of the hydraulic conductivity has been found.

References

[1] Bark, A.A., L.W. Gelhar, A.L. Gutjahr, and J.R. MacMillan. Stochastik analysis of spatial variability in subsurface flows,1, Comparison of one- and three- dimensional flows. *Water Resour. Res.*, 14(2), 263-271, 1978.

[2] Bellin A., Rinaldo A., Bosma W., van der Zee S., Rubin Y. Linear equilibrium adsorbing solute transport in physically and chemiacally heterogeneous porous formations. 1. Analytic solutions. *Water Resour. Res.*, 29, 4019-4031, 1993.

[3] Dagan G. Solute transport in heterogeneous porous formations. *J. Fluid Mech.*, 145, 151-177, 1984.

[4] G. Dagan. A note of the higher-order corrections of the head covariences in steady aquifer flow. *Water Resour. Res.*, 21, 573-578, 1985.

[5] G. Dagan. Flow and Transport in Porous Formation. Springer-Verlag. Berlin, Heidelberg, 1989.

[6] Freeze R.A. A stochastic-conceptual analysis of groundwater flow in non-uniform, homogeneous media. Water Resour. Res. 11(5), 725-741, 1975.

[7] Garabedian S.P., Gelhar L.W. and Celia M.A. Large-scale dispersivae transport in aquifers: Field experiments and reactive transport theory. Parsons Laboratory Report 315, MIT, Cambridge, 1988.

[8] Gelhar L.W., Gutjahr A.L. and Naff R.L. Stochastic analysis of macro-dispersion in a stratified aquifer. *Water Resour. Res.*, 19, 161-180, 1979.

[9] Gelhar, L.J., and C.L. Axness. Three-dimentional stochasic analysis of macrodispersion in aquifers. *Water Resour. Res.*, 19, 161-180, 1983.

[10] L.W. Gelhar. Stochastic Subsurface Hydrology. Englewood Cliffs, New Jersey: Prentice Hall, 1992.

[11] Kabala Z.J. and Sposito G. Stochastic model of reactive solute transport with time varying velocity in a heterogeneous aquifer. *Water Resour. Res.*, 27(3), 341-350, 1991.

[12] Kurbanmuradov and K.K. Sabelfeld. Lagrangian stochastic models for turbulent dispersion in the atmospheric boundary layer. *Boundary-Layer Meteorology*, vol.97 (2000), 2, 191-218.

[13] O.Kurbanmuradov, K. Sabelfeld and D. Koluhin. Stochastic Lagrangian Models for Two-Particle Motion in Turbulent Flow. Numerical Results. *Monte Carlo Methods and Applications*. (1997), V.3, N.3, 199-224.

[14] Kurbanmuradov O., Sabelfeld K., Smidts O. and Vereecken H. A Lagrangian stochastic model for the transport in statistically homogeneous porous media. WIAS Preprint N786, 2002.

[15] Matheron and de Marsily. Is transport in porous media always diffusive? A counter example. *Water Resour. Res.*, 16(5), 901-917, 1980.

[16] Metzger D., Kinzelbach H., Neuweiler I. and Kinzelbach W. Asymptotic transport parameters in a heterogeneous porous medium: Comparison of two ensemble-averaging procedures. *Stochastic Environmental research and Risk Assesment*, 13, 396-415, 1999.

[17] A.S. Monin and A.M. Yaglom. *Statistical Fluid Mechanics: Mechanics of Turbulence*, Volume 2. The M.I.T. Press, 1981.

[18] K.K. Sabelfeld. Monte Carlo Methods in Boundary Value Problems. New York, 1991.

[19] Sabelfeld and O.A. Kurbanmuradov. One-particle stochastic Lagrangian model for turbulent dispersion in horizontally homogeneous turbulence. *Monte Carlo Methods and Applications*, vol.4 (1998), N2, 127-140.

[20] L. Smith and R.A. Freeze. Stochastic analysis of steady state groundwater flow in a bounded domain, 1. One-dimensional simulation. *Water Resour. Res.*, 15(3), 521-528, 1979.